ELSEVIER

Journal of Volcanology and Geothermal Research 81 (1998) 173–187

Journal of volcanology and geothermal research

Thickness variations and volume estimates of tephra fall deposits: the importance of particle Reynolds number

C. Bonadonna, G.G.J. Ernst, R.S.J. Sparks *

Department of Earth Sciences, University of Bristol, Wills Memorial Building, Queen's Road, Bristol BS8 1RJ, UK

Received 12 March 1997; revised 18 November 1997; accepted 3 December 1997

Abstract

Well-preserved tephra fall deposits display thickness variations which are more complex than simple exponential thinning. On plots of log thickness against square root of area enclosed by an isopach contour, many deposits show two or more approximately straight-line segments and in some cases regions of curvature. We show that major changes in thinning rate occur as the particle size decreases with distance from the vent, as a consequence of the change of settling behaviour from high to low Reynolds number as predicted by W.I. Rose. Computer models of sedimentation from laterally spreading plumes predict a steep proximal segment with exponential thinning for coarse ejecta (lapilli and coarse ash) with high Reynolds number ($Re > 500$). At greater distance finer ejecta are predicted to show power-law thinning. Two distal segments are identified. The most distal segment is composed of low Reynolds number particles and can be approximated by an exponential thinning law, but is better described by a power law. The distal and proximal segments are connected by a curved segment containing mixed populations of intermediate ($0.4 < Re < 500$) and low Reynolds number particles ($Re < 0.4$). Many prehistoric tephra deposits are not preserved beyond the more proximal high Reynolds number segment and deposit volume, using a simple exponential thinning law, would be substantially underestimated if large amounts of ash were erupted. The database (number of defined isopach contours) is usually too sparse to recognise the intermediate region and curvature, so that the data will often be interpreted as two straight-line segments. The model predictions of break-in-slope distances for different column heights show good agreement with observed breaks-in-slope for eruption columns ranging from 12 to 45 km. Data indicate that the decay constant (the thickness half-distance b_t) for the proximal segment is also correlated with column height, as predicted by the models, and is only weakly dependent on total grain size distribution. Volcanic plumes rich in very fine ash (such as co-ignimbrite clouds) produce extensive deposits with large values of b_t.

Keywords: Reynolds number; tephra fall deposits; thickness

1. Introduction

The volume of tephra fall layers characterises the magnitude of an eruption. Various methods have been developed for estimating ejecta volumes from isopach maps (Rose et al., 1973; Walker, 1980, 1981a,b; Pyle, 1989, 1995; Fierstein and Nathenson, 1992) and this topic has caused some controversy (Rose, 1993; Fierstein and Nathenson, 1993). A major difficulty in estimating volumes is extrapolation beyond the preserved area of the deposit. Recent methods calculate volumes on the basis that expo-

* Corresponding author. Fax: +44-117-9253385; e-mail: steve.sparks@bristol.ac.uk

0377-0273/98/$19.00
PII S0377-0273(98)00007-9

nential thinning characterises the whole deposit (Pyle, 1989; Fierstein and Nathenson, 1992). Modelling of deposition of tephra from eruption columns (Sparks et al., 1992) provided theoretical support for an approximate exponential thinning law. However, tephra fall deposits have been documented with more complex thickness variations (e.g., Hildreth and Drake, 1992; Fierstein and Hildreth, 1992; Scasso et al., 1994). In particular when plotted on a diagram of log thickness (log T) against the square root of isopach area ($\sqrt{A}$), two or more approximately straight-line segments can occur. Although segmentation can be incorporated into volume estimates (Fierstein and Nathenson, 1992; Pyle, 1995), the origin of this segmentation has not been fully explained. Extrapolation of an empirical exponential thinning law beyond the preserved limits of a deposit is clearly unsafe if there is a possibility of a change in thinning rate.

In this paper we develop the sedimentation model of Sparks et al. (1992) to consider the influence of particle Reynolds number on thickness variation. The study by Sparks et al. (1992) assumed that particles settle by an inertial law at high Reynolds number. However, ash-sized particles (< 1 mm) typically show an increasing departure from the inertial law as grain size decreases and fine ash settles according to Stokes Law at low Reynolds number. Rose (1993) recognised that the different settling laws for coarse and fine particles might have an important influence on thickness variations. Hildreth and Drake (1992) and Fierstein and Hildreth (1992) also recognised that settling behaviour of fine ash caused differences between proximal and distal thinning rates.

Our study confirms these suggestions that a simple exponential law cannot be correct for eruptions containing significant sub-millimetre ash-sized ejecta and that extrapolation of exponential relationships to distances beyond the preserved limit is intrinsically unsound. Tephra layers are predicted to show two or more regions with contrasted thinning rates. We discuss a number of tephra fall deposits which confirm that the distal thinning rate of fine ash is quite different to the proximal thinning rate of lapilli and coarse ash. The majority of tephra fall deposits are only preserved in the proximal region so that the large difference between proximal and distal thinning is only apparent in exceptionally well-preserved deposits, most of which are historic events studied soon after the eruption.

2. Previous work and problems

Thorarinsson (1967) observed that tephra fall deposits from Hekla thinned exponentially. This observation has been confirmed by many studies since then. Pyle (1989) provided a systematic approach to the study of isopach maps by plotting data as the square root of the area enclosed by an isopach contour ($\sqrt{A}$) against the logarithm of the thickness (log T). He demonstrated that numerous deposits plot as straight lines on such a diagram. Thus tephra fall deposits could be characterised by a single decay constant and a thickness half-distance, b_t, could be defined. Integration of the exponential law enables a minimum volume of the deposit to be calculated (Fierstein and Nathenson, 1992; Pyle, 1995). Pyle (1989) recognised, however, that some deposits display two segments on a log T vs. $\sqrt{A}$ plot. Segmentation has been well-documented in some tephra deposits from historic eruptions (Hildreth and Drake, 1992; Fierstein and Hildreth, 1992; Scasso et al., 1994). Koyaguchi (1994) showed from mathematical analysis that the total grain size of the ejecta had to have specific distribution characteristics to produce an exponential decay law.

The approach of estimating volume by extrapolating the exponential thinning relations beyond the preserved thickness has been criticised by Rose (1993). His principal concerns were that volume estimates of some tephra deposits were much lower than those estimated by the crystal concentration method (introduced by Walker, 1980, 1981b) and that the fine distal ash may settle differently. Fierstein and Nathenson (1993) responded by pointing out significant problems with applying the crystal concentration method and observing that some tephra layers, for which the exponential method worked well were preserved to great distances and contained abundant fine ash. Below we show that these apparently different views can be reconciled, once the origin of the segmentation is understood.

Sparks et al. (1992) developed theoretical models of tephra deposition from the umbrella cloud of an eruption column in a still atmosphere based on a simple treatment of sedimentation from turbulent

suspensions (Martin and Nokes, 1988; Sparks et al., 1991). The model shows good agreement with data from rare eruptions in a weak wind (Bursik et al., 1992) and with laboratory experiments (Sparks et al., 1991). Some caution is required in applying these models to most tephra layers, because the wind is an important influence on dispersal in most eruptions. However, the models can be used to provide some important insights into tephra layer formation. In particular, for several different grain size distributions, numerical models of sedimentation predict approximate exponential thinning with b_t increasing with column height. Sedimentation models have also been developed for fallout of coarse ejecta from the margins of eruptions columns (Bursik et al., 1992; Ernst et al., 1996a). These studies predict a different sedimentation law within a few kilometres of the vent with a steeper decay rate and a marked break-in-slope at a distance corresponding to the corner of the eruption column, where the vertical buoyant plume reaches the neutral buoyancy level and then spreads laterally in the umbrella cloud. A number of deposits indeed show a very proximal break-in-slope (Pyle, 1989; Sparks et al., 1992; Hildreth and Drake, 1992).

There are problems with the above modelling work. Most tephra layers are only preserved in relatively proximal areas and are composed predominantly of lapilli and coarse ash. The modelling of Sparks et al. (1992) assumed that particles have terminal settling velocities governed by an inertial law in which the settling velocity is proportional to the square root of particle diameter. This law is valid for lapilli and coarse ash, but becomes increasingly incorrect for fine ash falling at low Reynolds number (Wilson and Huang, 1979; Rose, 1993). Further the boundary between low and high Reynolds number settling behaviour shifts to coarser grain sizes at higher altitudes in the atmosphere due to decreasing air density, making the influence of low Reynolds number fine particles greater for higher columns.

3. Observation of well-preserved tephra fall deposits

In this section we discuss observations of some exceptionally well-preserved tephra fall deposits that are not consistent with a simple exponential thinning law. Fig. 1 shows plots of log T vs. $\sqrt{A}$ for some of the tephra fall layers discussed here.

The 1980 Mount St. Helens plinian deposit shows a break-in-slope on a log T vs. $\sqrt{A}$ plot at about 27 km (Fierstein and Hildreth, 1992; Fig. 1a). This break-in-slope is too far from the volcano to be explained by the transition from column margin to umbrella cloud sedimentation. The distance between the column corner and the central plume axis is typically less than 30% of the column height. The height of the 1980 plinian column would imply that this transition only occurs at distances of 4 to 5 km from the vent. The '27 km' break-in-slope is, however, much closer to the source than the 'Ritzville' anomaly of secondary thickening observed beyond 300 km, which can be related to aggregation of fine ash (predominantly < 100 μm) (Sorem, 1982; Carey and Sigurdsson, 1982). Pyle (1989) also showed that the secondary maximum at Ritzville has no effect on the simple exponential thinning observed beyond $\sqrt{A} = 27$ km (Fig. 1a). The break-in-slope must therefore be due to another effect.

The 1932 Quizapú plinian deposit, Chile (Hildreth and Drake, 1992) and the various plinian units of the 1912 Novarupta eruption, Alaska (Fierstein and Hildreth, 1992) likewise display pronounced breaks-in-slope at values of $\sqrt{A}$ in the range of 7 to 105 km (Fig. 1a and b). In the case of Novarupta, Fierstein and Hildreth (1992) attributed the break-in-slope to the transition in sedimentation from the ascending plume to the umbrella region. However, except for one break-in-slope at $\sqrt{A} = 7$ km for Novarupta FGH, the distances are, as in the case of Mount St Helens, too great to be explained by this mechanism. Hildreth and Drake (1992) explained the Quizapú data as a consequence of a change in sedimentation mechanism for finer particles, suggesting that either aggregation or atmospheric turbulence caused the change.

The 1991 eruption of Mount Hudson, Chile, produced a tephra layer which extended across Argentina and is one of the best preserved and documented tephra deposit (Scasso et al., 1994). On a log T vs. $\sqrt{A}$ plot the deposit shows two prominent breaks-in-slope at $\sqrt{A} \approx 19$ and 57 km (Fig. 1a). The breaks-in-slope are again much too far away from the volcano to be explained by the transition from vertical column ascent to the umbrella cloud.

The AD180 plinian Taupo deposit (Walker, 1980) was formed from one of the most powerful plinian eruptions yet recognised, with an estimated column height of 51 km (Carey and Sparks, 1986). The plinian deposit displays approximate exponential thinning to distances of over 200 km. However, close inspection of the data (Fig. 1c) suggests that the data are better described by either two segments or slight curvature. Walker (1980) plotted up the individual thickness data on a log T vs. distance diagram and the data define a curve rather than a straight-line. Walker (1980) calculated that 83% of the ejecta in fact was deposited beyond the preserved area, using a mass balance method based on crystal content of the preserved deposit. However, this approach yields a much larger volume than is estimated by assuming the proximal exponential thinning relationship can be extrapolated to infinity. The discrepancy can be resolved if the fine distal ash layer thins much more gradually (Rose, 1993). The Hatepe deposit from Taupo also shows a break-in-slope at about $\sqrt{A} \approx 60$ km (Fig. 1c).

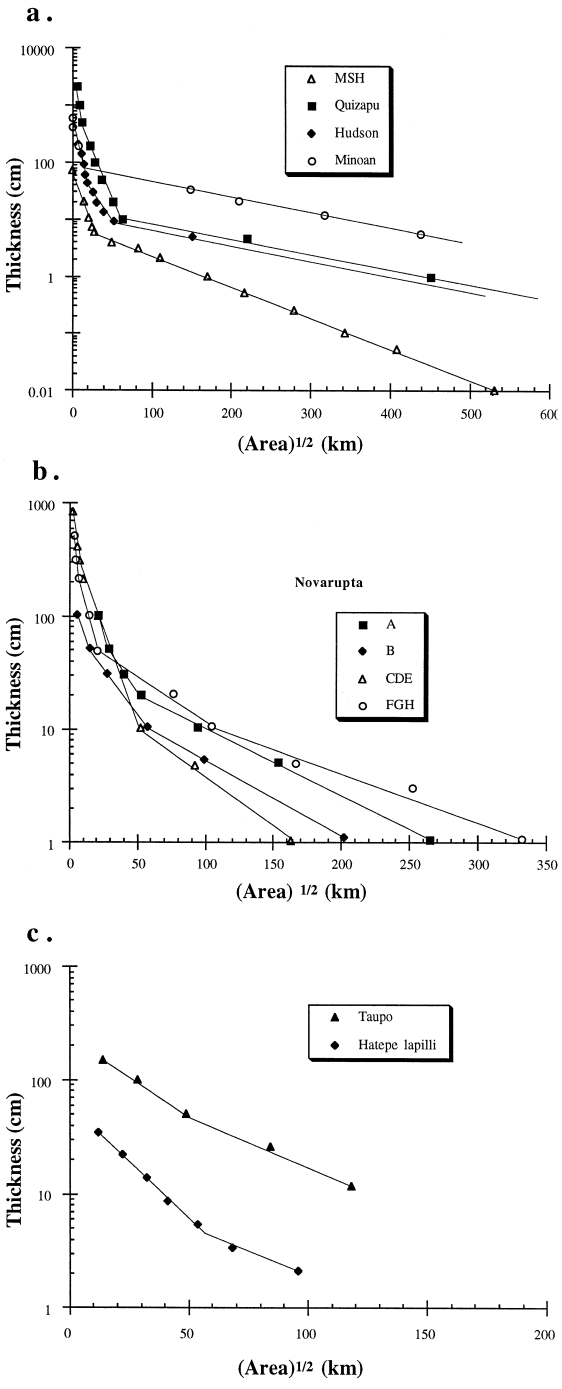

Fig. 1. Plots of log thickness (cm) against the square root of the area enclosed by an isopach map contour for some tephra fall deposits. (a) Data for the 1980 Mount St. Helens plinian deposit (after Carey and Sigurdsson, 1982), the Quizapú plinian deposit (after Hildreth and Drake, 1992), the 1991 Mount Hudson tephra (after Scasso et al., 1994) and the Minoan tephra of Santorini (after Pyle, 1989). (b) Data for tephra layers formed in the 1912 eruption of Novarupta (plot re-interpreted from the data of Fierstein and Hildreth, 1992). (c) Data for the Taupo plinian and Hatepe phreatoplinian deposits, New Zealand (after Walker, 1980).

4. Modelling

We develop the model of Sparks et al. (1992) to take account of the change of settling law from large particles falling at high Reynolds number to small particles falling at low Reynolds numbers. The model of Sparks et al. (1992) considers the umbrella cloud as a uniform turbulent suspension intruded as a gravity current into the atmosphere and calculates the relative mass flux of sedimenting particles as a function of distance. The model results reported by Sparks et al. (1992) do not properly describe the distal fallout, because the calculations used settling laws only appropriate at high Reynolds numbers.

We have adapted the model to calculate the Reynolds number of the particles and used the appropriate settling law depending on whether the Reynolds Number is high or low (See Kunii and Levenspiel, 1969: Chap. 3, Eqs. 29–31). At high Reynolds number terminal velocity is calculated as:

$$V_t \approx (3.1 g \rho d/\sigma)^{1/2} \quad (Re > 500) \tag{1}$$

where g is the gravitational acceleration, ρ is the particle density, d the particle diameter and σ the air density. For low Re number Stokes Law applies:

$$V_t \approx (g \rho d^2/18\mu) \quad (Re < 0.4) \tag{2}$$

where μ is the dynamic viscosity. At intermediate Reynolds number the terminal velocity can be approximated as:

$$V_t \approx d(4\rho^2 g^2/225\mu\sigma)^{1/3} \quad (0.4 < Re < 500) \tag{3}$$

The settling velocity depends on Reynolds number and therefore directly depends on atmospheric density for $Re \gg 0.4$. For a given particle size falling in the turbulent or transitional Re number regime the Reynolds number decreases and settling velocity increases with height as the atmospheric density decreases. Since the atmospheric density decreases exponentially with height, the boundaries between these three regimes vary with altitude (Fig. 2). Notice that the size of particles influenced by atmospheric viscosity ($Re < 500$) is greater for higher columns. At sea level the transitions occur approximately at 800–1200 μm ($Re = 500$) and 30–60 μm ($Re = 0.4$) depending on clast density (see Fig. 2), but at 40 km the transitions occur approximately at 3–10 mm ($Re = 500$) and 200–300 μm ($Re = 0.4$). Thus sedimentation of medium and fine ash must be influenced by atmospheric viscosity, a factor not taken into account in the previous study of Sparks et al. (1992).

Fig. 3 shows four model grain size distributions used here. Three of the size distributions have almost identical proportions of particles above 1 mm, all of which are expected to fall at high Reynolds number and therefore to give the same results as Sparks et al. (1992). The size distributions differ in the proportions of sub-millimetre ash which will, to a greater or lesser extent, be influenced by air viscosity. GS1 and GS2 are size distributions similar to those estimated for plinian eruptions (Sparks et al., 1992). GS3 is a size distribution largely containing high Reynolds number coarse particles to investigate the effects of having no sub-millimetre ash. GS4 is similar to the F3 tephra layer of the 1815 Tambora eruption (Sigurdsson and Carey, 1989) and is representative of a co-ignimbrite eruption plume with no coarse particles.

Fig. 4a shows calculations of thickness variation with distance for different column heights (10 to 50 km) using distribution GS2 and assuming a particle density of 750 kg m^{-3}. In the calculations S is the mass flux of sedimenting particles per unit area and S_o is the mass flux at the origin. For a constant column height, mass flux is proportional to deposit thickness (see Sparks et al., 1992), so that $\ln S/S_o$ is a proxy for the log of the thickness. The results show that the thickness variations are not a simple exponential.

We have identified for each model three distinct segments on $\ln T$ vs. $\sqrt{A}$ plots (Fig. 4b) based on the proportions of particles with different Reynolds number at different distances. These three segments are referred to as Seg_1, Seg_2 and Seg_3. The proportion of particles in the three categories ($Re > 500$, $0.4 < Re < 500$ and $Re < 0.4$) are shown as a function of distance for a typical calculation (Fig. 5) and demonstrate that the segmentation is simply a consequence of different sedimentation laws dominating in proximal and distal regions. The proximal straight-line segment, Seg_1, represents the region where lapilli and coarse ash are deposited at high Reynolds number and its limit is defined by the distance at which the proportion of high Reynolds number particles falls to near zero. This segment is well approximated by exponential thinning. Segment Seg_3 is defined beyond the distance where more than 60% of particles have $Re < 0.4$. Seg_3 is not precisely a straight-line, showing slight curvature (Fig. 4b). The distal segment Seg_3 represents the deposition of medium and fine ash at low Reynolds number. The occurrence of the distal segment is more prominent for the higher columns (Fig. 4a). This is a consequence of the decrease in density of the atmosphere with height, which results in a higher proportion of the ejecta, for a given size distribution, being in the intermediate and low Reynolds number category (Fig. 2). The segment Seg_2 between the high and low Reynolds number segments is composed of a mixture of mostly

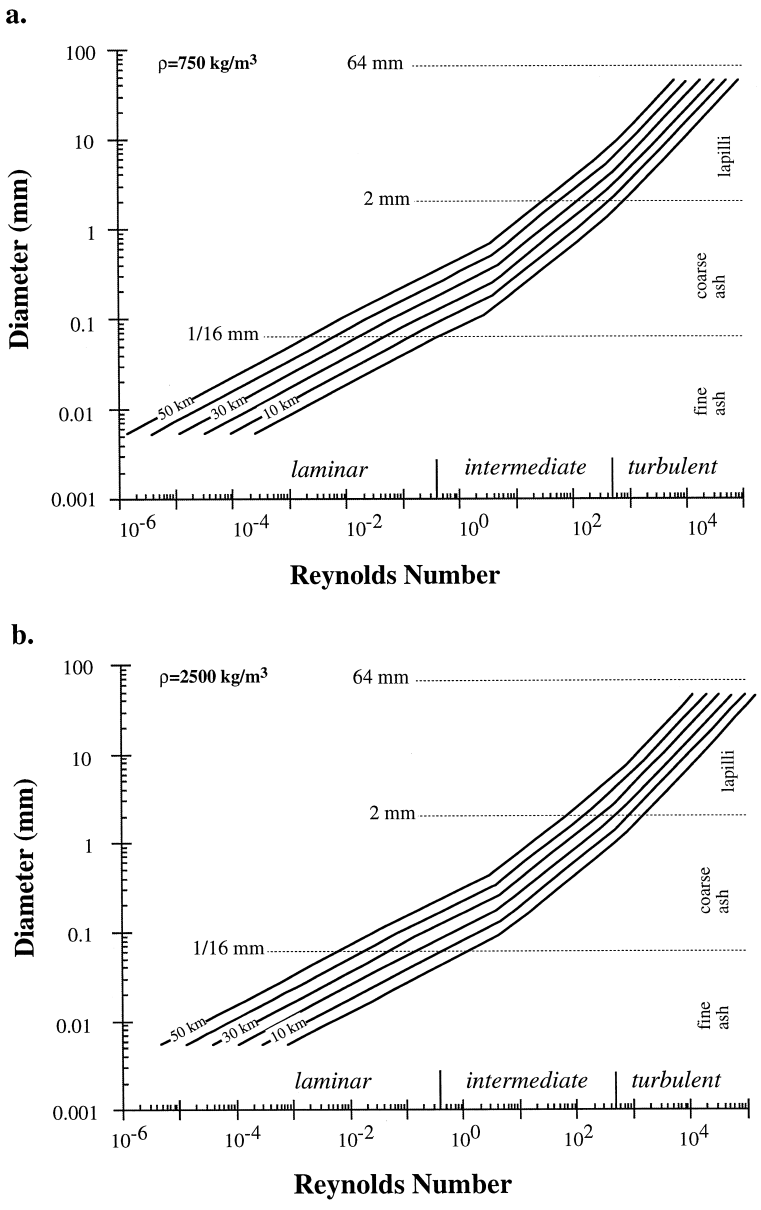

Fig. 2. A plot of particle Reynolds number against particle diameter for different altitudes in the atmosphere. Note that the transitions between high, intermediate and low Reynolds number increases in grain size with altitude in the atmosphere. (a) and (b) are for typical densities of pumices and lithics, 750 and 2500 kg m^{-3} respectively.

intermediate and low Reynolds number particles (Fig. 5). Segments 2 and 3 together define a continuous gently curved region. The average Reynolds number of the deposited particles decreases with distance resulting in a decrease in thinning rate.

Fig. 6 shows model calculations for the same column height (30 km) and four different grain size distributions. The particle density is assumed to be 750 kg m^{-3} for GS1, GS2 and GS3, but is assumed to be 2000 kg m^{-3} for GS4, to simulate fallout of

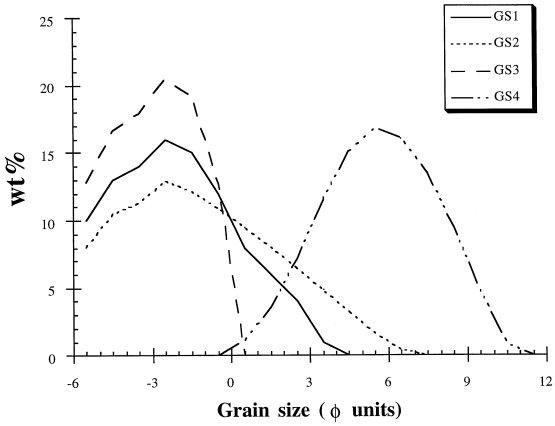

Fig. 3. Model grain size distributions used in modelling. Note that the relative proportions of coarse particles greater than 1 mm in diameter ($Ø = 0$) are the same in each distributions GS1, GS2 and GS3 whereas GS4 is much finer (based on the size distribution for one of the 1815 Tambora co-ignimbrite ash fall deposit, F3, after Sigurdsson and Carey, 1989).

dense glass shards and crystals expected in a co-ignimbrite plume. The result for the distribution with no sub-millimetre ash (GS3) shows a single approximately exponential segment. The two distributions with both coarse and fine particles (GS1 and GS2) show the three segments. The distal segment is more pronounced for distributions with larger proportions of sub-millimetre ash (GS2 and GS4). The proximal segments are almost identical for the three cases with coarse ejecta (GS1, GS2 and GS3). If the proximal segments were only preserved, then the three deposits would have identical exponential decay constants, but the actual ejecta volume would differ by a factor of 2 between GS2 and GS3. In the examples with significant sub-millimetre ash extrapolation of the proximal segment would be invalid.

Comparison of the distal segments of GS2, GS3 and GS4 shows that the thinning rate is quite sensitive to the size distribution of low Reynolds number particles. If the slightly curved distal low Reynolds number segment is approximated by an exponential law (see Fig. 4b), then b_t increases as the proportion of finer-grained particles in the initial distribution increases. This contrast can be explained in terms of the range of settling velocities. High Reynolds number particles have a much narrower range of settling velocities than low Reynolds number particles, because of the much stronger dependence on particle diameter of the latter. Thus low Reynolds number particles have a much wider range of settling velocities making the thinning rate more sensitive to the size distribution.

Thickness variations in the distal areas of deposition of intermediate and low Reynolds number particles are better described by power law functions.

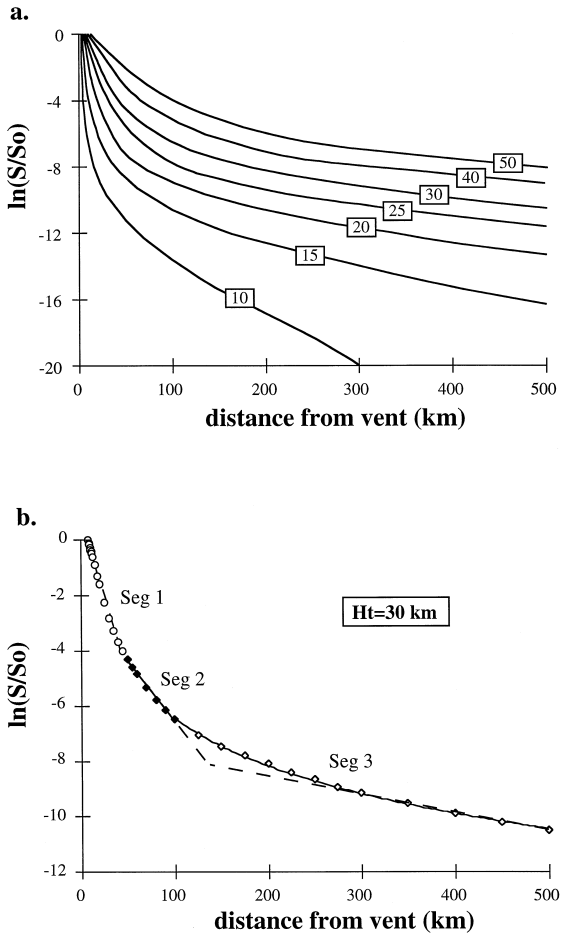

Fig. 4. Variation of relative mass sedimentation flux ($\ln S/S_o$) against radial distance from the vent. Clast density is taken as 750 kg m^{-3} (a) Model calculations for grain size distribution GS2 for column heights from 10 to 50 km. (b) Model calculation for grain size distribution GS2 for a column height of 30 km showing individual calculated points. The points have been given three different symbols to show the proximal, intermediate and distal segments, based on the proportion of different Reynolds number particles. The three segments are labelled Seg_1 to Seg_3.

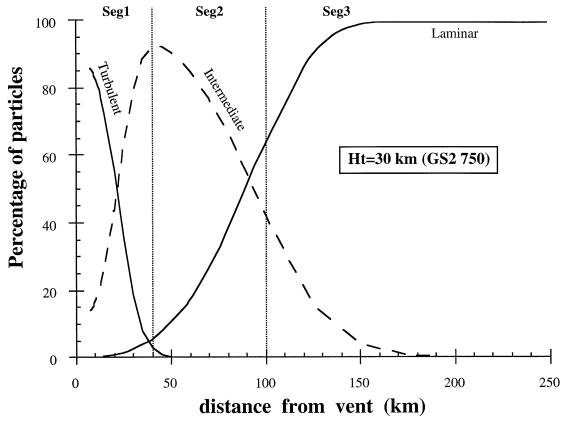

Fig. 5. The proportions of high, intermediate and low Reynolds number particles in the deposit are shown as a function of distance from the source for a model calculation for GS2 size distribution and a column height of 30 km. The diagram links in with Fig. 4. Clast density is taken as 750 kg m^{-3}.

Fig. 7 shows model calculations for GS4 (Fig. 7a). GS4 does not show Seg_1 at all as it is characterised by particles with $Re < 500$ only. Thus GS4 plots show Seg_2 and Seg_3 only (segments controlled by intermediate and low Re number particles). So the GS4 case gives the opportunity to better analyse the power law behaviour (Fig. 7b), showing that the exponent is a linear function of column height (Fig. 7c). The power law exponent approaches unity for high columns, with curvature becoming greater for

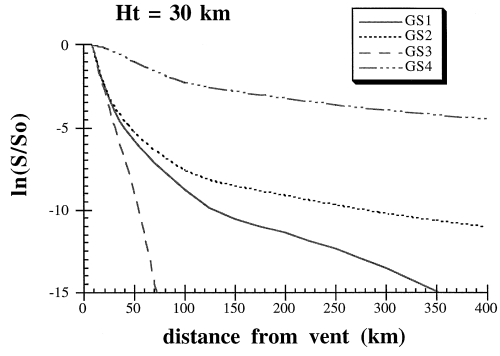

Fig. 6. The variation of relative mass flux ($\ln S/S_o$) vs. distance for a column height of 30 km modelled for four different grain size distributions (see Fig. 3). The proximal straight-line segments are indistinguishable for the three model distributions containing coarse particles. The particle density is taken as 750 kg m^{-3} for GS1, 2 and 3 and 2000 kg m^{-3} for GS4.

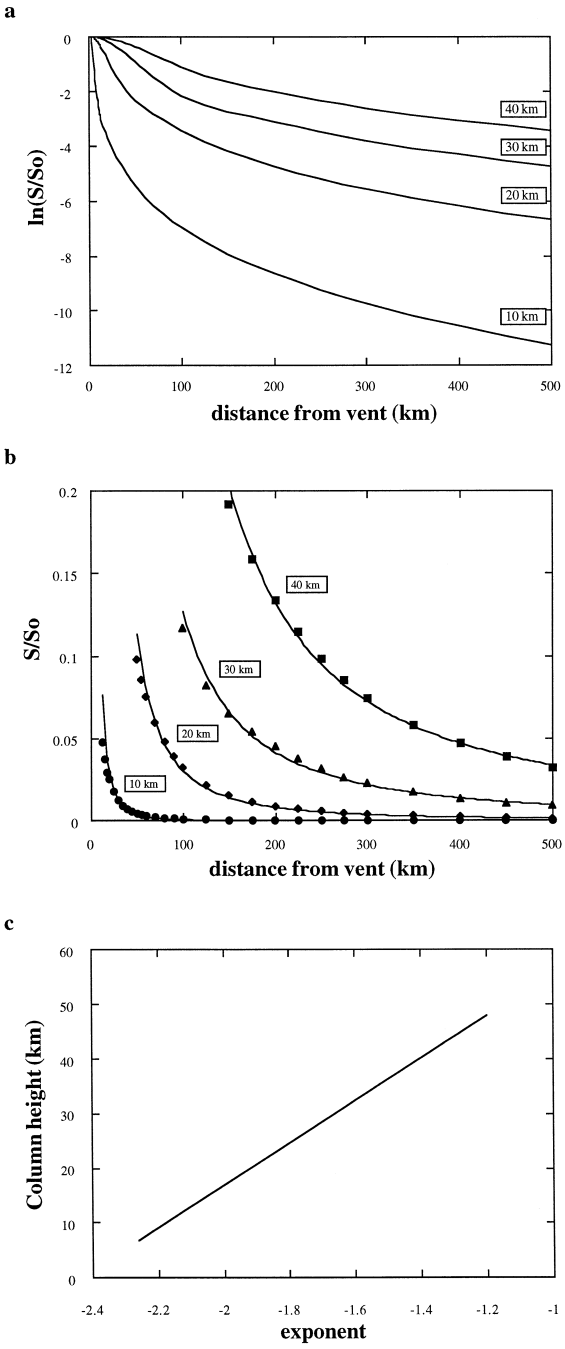

Fig. 7. Model calculations for GS4 grain size distribution. (a) The thickness vs. distance relationship for four different column heights. (b) Power law fits to calculated points for segment Seg_3. (c) The power law exponent plotted against column height.

lower columns. Thus an exponential approximation is better for higher columns.

The models are strictly valid for the no-wind case, but, provided results are compared to data plotted on a $\sqrt{A}$ basis, semi-quantitative comparison with wind-blown deposits is possible. The physical principles of a change of settling law, which accounts for segmentation, remain valid and will be a fundamental feature of wind-blown plumes. Expressing isopach data as the square root of the area as a normalisation procedure reduces the distorting effects of the wind, which changes the shape of a thickness contour, but has little effect on the area enclosed (Pyle, 1989). Comparison of models with data, discussed below, justify the application a posteriori.

The comparison between models and data cannot be very precise for several reasons. First, the calculations assume a single particle density and tephra deposits contain particles with a wide range of densities and shapes. The irregular shape of ash particles also can result in significantly lower fall velocities than spherical particles of equivalent volume (Wilson and Huang, 1979). Second, in a wind-field fine particles are completely removed from proximal areas, whereas the models in the absence of wind have sedimentation of fine particles at all distances. Until models are developed which incorporate the wind, it is unclear how important the wind will be on the relationships between column height, grain size distribution and area enclosed by isopach contours. Third atmospheric turbulence can further reduce the settling velocity of fine particles (Stout et al., 1995). Finally particles below 1 μm in diameter will be influenced by molecular motions reducing the settling velocity below Stokes law values. All these factors will tend to increase the dispersal of fine ash. On the other hand aggregation of ash causes a decrease in dispersal of fine ash (Sorem, 1982; Carey and Sigurdsson, 1989).

5. Discussion

The theoretical calculations show that simple exponential thinning is not expected for eruptions which generate significant amounts of sub-millimetre ash as well as lapilli and coarse ash. Coarse particles fall by an inertial settling law independent of air viscosity and proportional to the square root of the particle diameter. Sedimentation generates an approximately exponential decay in thickness until the proportion of particles with $Re > 500$ becomes negligible at which point thinning is better described by a power law than by exponential thinning. Medium and fine ash particles fall with intermediate or low Reynolds number influenced by atmospheric viscosity and have settling velocities which depend either on particle diameter or the square of the diameter. Distal regions of the deposit show much reduced thinning rates.

The models predict that changes in the thinning rate and ejecta grain size distribution are linked. In the models departure from the proximal exponential decay segment initiates at values of $\ln(S/S_o)$ of about -5. This corresponds to a thickness slightly less than the 0.01 T_{max} parameter that Walker (1973) used to define the dispersal index (D). Here T_{max} is the maximum deposit thickness and D is the area enclosed by the 0.01 T_{max} isopach contour. $\ln(S/S_o) = -5$ corresponds to about 0.006 T_{max}, if it is assumed that the maximum thickness is that estimated by extrapolating back the straight-line segment to source. The choice of 0.01 T_{max} by Walker (1973) was pragmatic in that many prehistoric tephra fall deposits are not well preserved much beyond 0.01 T_{max}. Similarly, a dataset of total grain size distributions from plinian deposits (Walker, 1981a) show that almost all samples are greater than 0.5 mm in median diameter. Thus, preserved parts of most prehistoric plinian deposits are composed of lapilli and coarse ash and are only expected to show the high Reynolds number proximal straight-line segment. We suggest that it is an artefact of preservation that many tephra fall deposits display simple exponential thinning (Pyle, 1989).

5.1. Volume calculations

The consequences of the change in slope for volume estimates are clear. Use of the method of Pyle (1989, 1995) or Fierstein and Nathenson (1992) with a thickness half-distance derived from the commonly preserved regions of tephra fall deposits can only give a minimum volume. The amount that the volume is underestimated depends on the proportion of sub-millimetre ash. If the proportion of ash is

substantial, as is the case for 1980 Mount St. Helens, AD180 Taupo and 1991 Mount Hudson deposits, then the true volume may be much larger, in agreement with volume estimates based on the crystal concentration method (Rose, 1993). Unfortunately the models suggest that there is no information in the proximal thickness variations to constrain the proportion of distal fines (Fig. 6). Other methods, such as the crystal concentration study of Walker (1981a,b), are required to obtain volume estimates if there is no preserved distal tephra. This method, however, may overestimate the volume if there are significant amounts of accidental (non-juvenile) crystals which cannot be easily distinguished from juvenile crystals, and there are other problems, as identified by Fierstein and Nathenson (1993).

The differing views of Rose (1993) and Fierstein and Nathenson (1993) can, to some extent, be reconciled. If for example plinian deposits similar to 1980 Mount St. Helens or Quizapú were only preserved to 30 and 60 km, respectively then only the proximal high Reynolds number segment would be available and application of the methods of Pyle (1989) and Fierstein and Nathenson (1992) would greatly underestimate the true volume. This indeed is the situation for many ancient deposits or those on island volcanoes. On the other hand, for well-preserved deposits showing both the high and low Reynolds number segments, application of these methods should give fairly good volume estimates. Fierstein and Nathenson (1993) give convincing arguments that there will be only minor amounts of ultra fine ash deposited beyond the limits of well-preserved deposits like Mount St. Helens.

5.2. Comparison of models with observations

Fig. 8 and Table 1 show a comparison between the model calculations with the 1932 Quizapú and 1991 Mount Hudson deposits. The calculations were made for a single particle density (750 kg m^{-3}) with grain size distribution GS2 for the mean estimated column height of each eruption. The agreement is encouraging with the change of thinning rate between proximal and distal regions being comparable. If the thickness variations are approximated as straight-line segments, then the values of b_t are similar for models and observations (Table 1). There

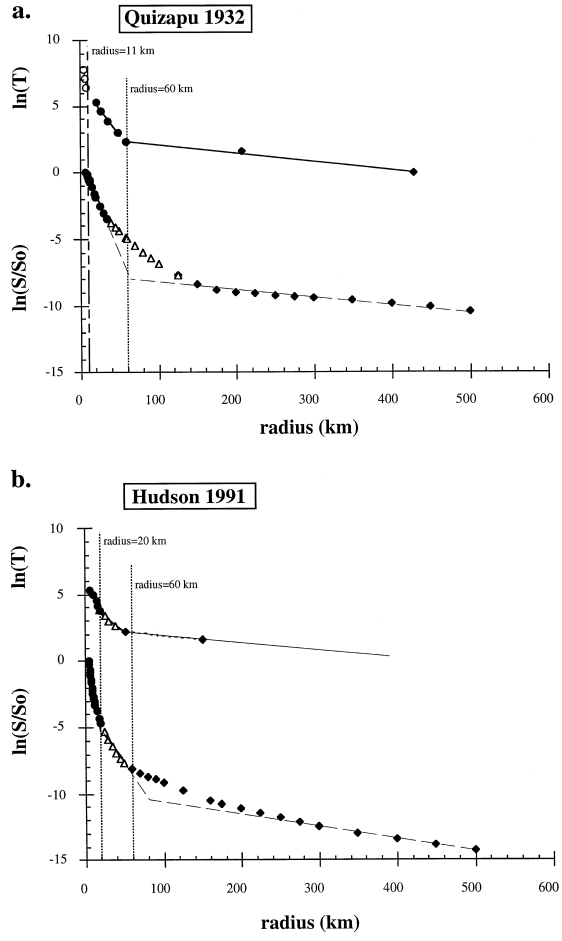

Fig. 8. Comparison between data for two historic tephra layers (Hildreth and Drake, 1992; Scasso et al., 1994) and the models (considering $H_t = 28.5$ and 18 km, respectively; distribution GS2 and $\rho = 750$ kg m^{-3}): (a) Quizapú, 1932 and (b) Mount Hudson, 1991. Radius represents square root of isopach area for the tephra layers and distance from vent for the models. The three segments (Seg_1, Seg_2 and Seg_3) are denoted by different symbols. In the case of the Quizapú eruption (Fig. 8a) data points to the left of the 11 km break-in-slope are not taken into account in the model calculations presented here as they are thought to correspond to sedimentation from the plume margins.

is, however, some subjectivity in choosing which data or calculated points to include in the straight-line fits, particularly in the distal segments which show curvature. There are also detailed differences, in particular the intermediate segment Seg_2 is not clear in the deposit data. The representation of the distal data as a straight-line is also an artefact of the small

Table 1
Comparison between observed (published) data and predictions by the model, for the 1932 Quizapú and 1991 Hudson cases

		Breaks-in-slope	b_{t1}	b_{t2}	b_{t3}	wt.% < 1 mm		wt.% < 63 μm	
						58 km	200 km	58 km	200 km
1932 Quizapú	observed	58	5.4	62.4		99.6	100	2.6	0.5
	predicted	64(v)	5.1	14.8	78.3	82.0	100	64.5	30.0

		Breaks-in-slope	b_{t1}	b_{t2}	b_{t3}	wt.% Re < 500		wt.% Re < 0.4	
						57 km	160 km	57 km	160 km
1991 Hudson	observed	19, 57	3.1	8.5	62.5	97	100	27	91
	predicted	20, 55	2.2	8.0	71.9	100	100	81	100

(v): Virtual break-in-slope, i.e., break-in-slope obtained by extrapolating Seg_1 and Seg_3.
Values of b_t are estimated for the three segments in the natural deposits and compared with the predicted model values. Beyond Seg_o, only two segments can be recognised in the Quizapú deposit. The break-in-slope between segments is estimated by finding the intersection between the two neighbouring segments. b_{t2} observed has to be compared with b_{t3} predicted in the case of Quizapú. The predicted and observed wt.% of particles $<$ 1mm and $<$ 63 μm is given for the Quizapú deposit at two different distances. The predicted and observed wt.% of particles with Re $<$ 500 and Re $<$ 0.4 are given for the Hudson deposit at two different distances. b_t values are obtained from $b_t = (\ln 2)/(k\pi^{1/2})$ for published plots of ln(Thickness) vs. (Isopach Area)$^{1/2}$ (see Pyle, 1989) and using $b_t = (\ln 2)/k$ for the plots of $\ln(S/S_o)$ vs. distance from vent predicted by the theory.

number of isopach contours. The subtle power-law curvature in the models may simply be beyond the resolution of typical field data to detect. A possible reason for the absence of a clear segment Seg_2 is the effect of wind. Recent experiments on fallout from plumes in a crossflow suggest that fine particles may be completely detached from source by the wind, enhancing the separation of high and low Reynolds number particles (Ernst et al., 1996b). Given the differences between the field data and the models, we conclude that the comparison is sufficiently good to demonstrate that the thickness variations can largely be explained in terms of particle Reynolds number.

The modelling predicts that the decrease in thinning rate with distance should be linked to regions of the deposit where significant amounts of intermediate and low Reynolds number particles (medium and fine ash) begin to appear. This is the case in the examples of exceptionally well-preserved deposits. Table 1 compares grain size data and model predictions at the distal break-in-slope and beyond for well-preserved deposits confirming this expectation.

The distance from vent to the break-in-slope between the high and low Reynolds number segments increases with column height (Fig. 4a). This prediction can be tested against observations. However, some difficulties arise in the comparison. A source of discrepancy between the predicted and observed thickness decay trends is due to the difference in the dataset interval available. In our computer model, a suitably large interval of radial distances (0 to 500 km from the vent) has been considered in order to study the mass decay trend from the very proximal to the distal region. In contrast, isopach contour datasets may not be complete enough to define entirely the trend expected from the theory. This problem is accentuated by the fact that the expected trend is characterised by a curved rather than a straight line. Thus the distance at which breaks-in-slope occur also depends on which interval of radial distances has been considered. The discrepancy is illustrated in Table 2 where observed data are compared to predicted values derived either for an interval of radial distances identical to that of the observed datasets or for a 0–500 km interval thought to correspond to a fairly ideal dataset.

As illustrated on Fig. 9a, predicted values (both break-in-slope distances and b_t values) fit the observed data well when the same radial distance interval is considered. Fig. 9b shows the excellent correlation between H_t and the distance to the break-in-slope derived based on a suitably large interval of radial distances (0–500 km), but a much poorer

Table 2
Comparison between observed and predicted breaks-in-slope and b_t values

Deposit	Mean H_t (km)	Data set interval (km)	Breaks-in-slope (1–2)		b_{t2}	
			Obs	Pred	Obs	Pred
1. Hekla 1970, Iceland	12	3–90	10	12.5	7.8	7.8
		0–500		7.0		2.2
2. Hudson 1991, Chile	18	0–160	19	15.0	8.5	6.5
		0–500		20.0		8.0
3. Mt. St. Helens (18 May 1980)	19	0–500	27	34(v)	31	69.3(v)
				20.0		8.3
4. Novarupta FGH (1912), Alaska	20	0–350	21	20.0	22	9.2
		0–500		20.0		8.3
5. Novarupta CDE (1912), Alaska	23	0–170	52	27.0	18.8	11.6
		0–500		30.0		10.8
6. Apoyo A, Nicaragua	23	8–41	27	22.0	7.1	7.9
		0–500		30.0		10.8
7. Novarupta A (1912), Alaska	25	0–270	30	27.5	10.2	11.2
		0–500		30.0		12.4
8. Novarupta B (1912), Alaska	25	0–200	16	27.5	10.3	11.9
		0–500		30.0		12.4
9. Quizapú 1932, Chile	28.5	0–450	58	64(v)	62.4	78.3(v)
				35.0		14.8
10. Pinatubo 1991, Philippines	33	11–500	94	80(v)	94.7	94.9(v)
		(gap 40–300)		50.0		18.2
11. Hatepe pumice, New Zealand	33	20–100	61	55.0	16.2	17.3
		0–500		50.0		18.2
12. Waimihia, New Zealand	42	12–112	59	57.0	12.2	19.6
		0–500		65.0		25.8
13. Los Chocoyos, Guatemala	45	33–1450	101	125.0	13.4	17.9
		0–500		65.0		26.6

References for H_t data: 1. Thorarinsson and Sigvaldason, 1972; Scasso et al., 1994; 3. Carey and Sigurdsson, 1989; 4, 5, 7 and 8. Fierstein and Hildreth, 1992; 6. authors' calculation; 9. Hildreth and Drake, 1992; 10. Paladio-Melosantos et al., 1996; 11, 12 and 13. Carey and Sigurdsson, 1989. References for b_t and breaks-in-slope from plots of log T vs. $\sqrt{A}$ (breaks-in-slope between Seg_1 and Seg_2 are considered in this table as they are the most frequently observed in studied deposits): 1, 2, 4, 5, 7, 8 and 9: authors' calculations from published data (see above); 10: authors' calculation based on Paladio-Melosantos et al. (1996) and Wiesner et al. (1995); 3, 6, 11, 12 and 13: Fierstein and Nathenson, 1992.

correlation between H_t and the observed distances to the break-in-slope, which are typically determined from deposits preserved over a limited interval of radial distances. These considerations confirm the predictive potential of the model but highlight limitations inherent to the incomplete preservation of field deposits. We found, however, a good correlation between H_t and the distance to the observed break-in-slope when the distal break-in-slope is derived by extrapolating the most proximal and the most distal data points. The correlation, displayed on Fig. 10, corresponds to the empirical relationship:

$$H_t(\text{km}) \approx 12 + 0.3\sqrt{A_{BS}} \quad (\text{for } 12\,\text{km} < H_t < 45\,\text{km}) \tag{4}$$

which offers a simple practical method to estimate H_t to within 20% from the determination of the distal break-in-slope in field data.

Models of tephra sedimentation (Sparks et al., 1992) indicate that the thickness half-distance can also be related to eruption column height. Fig. 11 shows the theoretical relationship predicted between column height and thickness half-distance and data from some tephra fall deposits. Values of b_t derived from the proximal lapilli and coarse ash region of the deposits show approximate agreement with theory, noting however the caveat that the effect of wind on b_t is not yet known, although it is not expected to cause major changes (Pyle, 1989; Sparks et al., 1992).

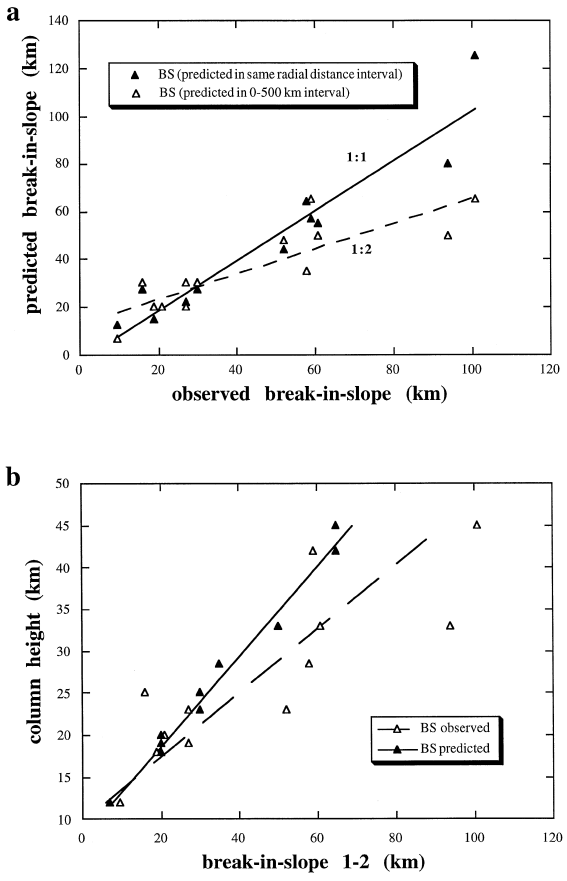

Fig. 9. (a) The theoretical break-in-slope is plotted against the observed break-in-slope. Data are given in Table 2. Solid triangles represent break-in-slope values determined for theoretical curves extending over the same interval of radial distances as the corresponding field data for each of the deposits considered; open triangles represent break-in-slope values determined from the theoretical curves and a large interval (0–500 km) of radial distances. Regression lines through the data, characterized by 1:1 and 1:2 slopes, respectively are showed. (b) The mean eruption column height (either observed or calculated by the method of Carey and Sparks, 1986) is plotted both against the position of the break-in-slope predicted (over a interval of radial distances of 0–500 km) and that of the observed break-in-slope. Solid and open triangles represent predicted and observed breaks-in-slope, respectively.

A final consequence of this study concerns interpretation of distal tephra deposits as co-ignimbrite fall deposits. The change in thickness variation with distance, as observed for example in the Mount Mazama tephra, has been interpreted as a change from plinian to co-ignimbrite ash deposition (Sparks

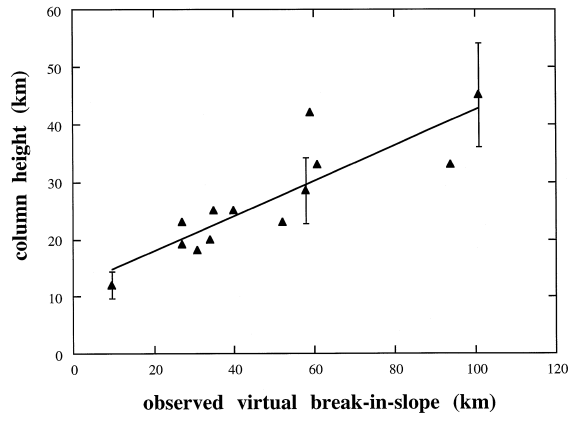

Fig. 10. The eruption column height (either observed or estimated by the method of Carey and Sparks, 1986) is plotted against the observed position of the break-in-slope obtained by extrapolating the trends defined by the most proximal and the most distal data points (observed virtual break-in-slope). H_t is typically estimated to within 20% (see Carey and Sparks, 1986) and 20% error bars are illustrated for three data points for low, intermediate and high columns, respectively.

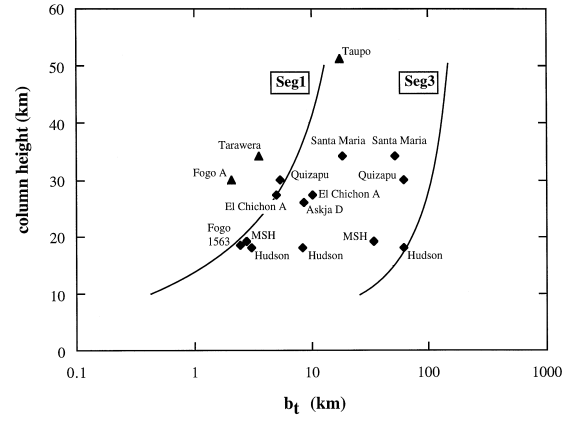

Fig. 11. The theoretical relationship between thickness half-distance, b_t, and column height, H_t, is shown for both the proximal high Reynolds number segment (Seg_1) and distal low Reynolds number segment (Seg_3). Observations are also plotted: as triangles, for cases with a single segment on plots of ln (Thickness) vs. (Isopach Area)$^{1/2}$, and diamonds for cases with two or three segments on such plots (i.e., several b_t values and diamonds). Only b_t values for segments beyond the plume corner distance are plotted. Several deposits have more than one segment resulting in multiple b_t values for the same event.

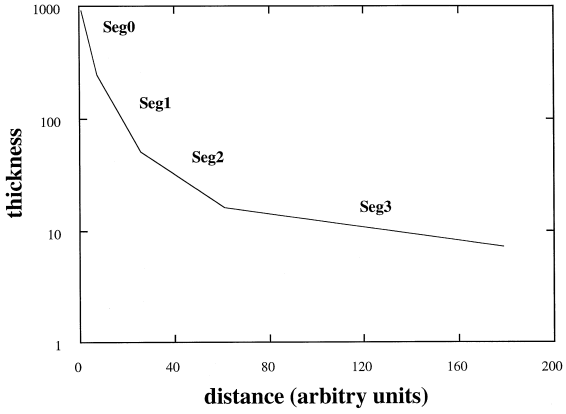

Fig. 12. Generalized model for the thickness variations in a tephra fall deposit on a ln T vs. $\sqrt{A}$ plot showing segmentation, as described in the text.

and Walker, 1977; Sparks and Huang, 1980). However, our study negates this as a convincing argument as the change can also be explained as a simple regime change in the hydrodynamic settling of particles from proximal to distal regions. Izett (1981) argued that many distal ash from large magnitude explosive eruptions present distal co-plinian deposits rather than co-ignimbrite ash. There are other arguments, however, for believing that larger magnitude ignimbrite eruptions generate substantial proportions of distal co-ignimbrite ash. Our study also indicates that large values of b_t are a characteristic feature of co-ignimbrite ash layers.

The results of the modelling work in this and related papers (Bursik et al., 1992; Sparks et al., 1992; Ernst et al., 1996a) suggest a generalised model of thickness variations in tephra fall deposits (Fig. 12). The very proximal segment, Seg_o, is related to fallout from the column margins whereas three more segments (Seg_1, Seg_2 and Seg_3) are related to fallout from the umbrella cloud. The proximal segment, Seg_1, is formed from deposition of high Reynolds number particles. The curved segment, Seg_2, is a transitional region where a mixed population of high, intermediate and low Reynolds number particles are deposited. The distal segment, Seg_3, is formed from deposition of low Reynolds number particles. An accurate estimate of volume requires all four segments to be preserved.

Acknowledgements

C. Bonadonna was supported by the Erasmus programme. G.G.J. Ernst was supported by the EC and the 'Fondation Belge de la Vocation' and NERC (BRIDGE grant 31). R.S.J. Sparks was supported by the Leverhulme Trust (grant F/192/AL). Mauro Rosi is thanked for supporting the visit of C. Bonadonna to Bristol. Reviews by J. Fierstein and W.I. Rose are acknowledged.

References

Bursik, M.I., Sparks, R.S.J., Gilbert, J.S., Carey, S.N., 1992. Sedimentation of tephra by volcanic plumes: I. Theory and its comparison with a study of the Fogo A plinian deposit, Sao Miguel (Azores). Bull. Volcanol. 54, 329–344.

Carey, S.N., Sigurdsson, H., 1982. Influence of particle aggregation on deposition of distal tephra from the May 18, 1980, eruption of Mount St. Helens Volcano. J. Geophys. Res. 87, 7061–7072.

Carey, S.N., Sigurdsson, H., 1989. The intensity of plinian eruptions. Bull. Volcanol. 51, 28–40.

Carey, S.N., Sparks, R.S.J., 1986. Quantitative models of the fallout and dispersal of tephra from volcanic eruption columns. Bull. Volcanol. 48, 109–125.

Ernst, G.G.J., Carey, S.N., Bursik, M.I., Sparks, R.S.J., 1996a. Sedimentation from turbulent jets and plumes. J. Geophys. Res. 101, 5575–5589.

Ernst, G.G.J., Palmer, M.R., Sparks, R.S.J., German, C.R., 1996b. Fallout from hydrothermal and volcanic plumes in crossflow: experimental data and new models. Eos Trans. AGU 77, 815, supplement.

Fierstein, J., Hildreth, W., 1992. The plinian eruptions of 1912 at Novarupta, Katmai National Park, Alaska. Bull. Volcanol. 54, 646–684.

Fierstein, J., Nathenson, M., 1992. Another look at the calculation of fallout tephra volumes. Bull. Volcanol. 54, 156–167.

Fierstein, J., Nathenson, M., 1993. Bull. Volcanol. 55, 375–378, Reply to the comment by W.I. Rose.

Hildreth, W., Drake, R.E., 1992. Volcano Quizapu, Chilean Andes. Bull. Volcanol. 54, 93–125.

Izett, G.A., 1981. Volcanic ash beds: recorders of Upper Cenozoic silicic pyroclastic volcanism in the Western United Sates. J. Geophys. Res. 86, 10200–10222.

Koyaguchi, T., 1994. Grain-size variations of tephra derived from volcanic umbrella clouds. Bull. Volcanol. 56, 1–9.

Kunii, D., Levenspiel, O., 1969. Fluidisation Engineering. Wiley, New York.

Martin, D., Nokes, R., 1988. Crystal settling in a vigorously convecting magma chamber. Nature 332, 534–536.

Paladio-Melosantos, M.L., Solidum, R., Scott, W.E., Quiambo,

R.B., Umbal, J.V., Rodolfo, K.S., Tubianosa, B.S., Delos Reyes, P.J., 1996. Tephra falls of the 1991 eruptions of Mount Pinatubo. In: Newhall, C.G., Punongbayan, R.S. (Eds.), Fire and Mud: Eruptions and Lahars of Mount Pinatubo, Philippines. PHILVOLCS and Univ. of Washington Press, 1126 pp.

Pyle, D.M., 1989. The thickness, volume and grainsize of tephra fall deposits. Bull. Volcanol. 51, 1–15.

Pyle, D.M., 1995. Assessment of the minimum volume of tephra fall deposits. J. Volcanol. Geotherm. Res. 69, 379–382.

Rose, W.I., 1993. Comment on 'Another look at the calculation of the fallout tephra volumes' by Fierstein, J., Nathenson, M., Bull. Volcanol. 59: 372–374.

Rose, W.I., Bonis, S., Stoiber, R.E., Keller, M., Bickford, T., 1973. Studies of volcanic ash from two recent Central American eruptions. Bull. Volcanol. 37, 338–364.

Scasso, R., Corbella, H., Tiberi, P., 1994. Sedimentological analysis of the tephra from the 12–15 August 1991 eruption of Hudson Volcano. Bull. Volcanol. 56, 121–132.

Sigurdsson, H., Carey, S.N., 1989. Plinian and co-ignimbrite tephra fall from the 1815 eruption of Tambora Volcano. Bull. Volcanol. 51, 143–270.

Sorem, R.K., 1982. Volcanic ash clusters: tephra rafts and scavengers. J. Volcanol. Geotherm. Res. 13, 63–71.

Sparks, R.S.J., Huang, T.C., 1980. The volcanological significance of deep-sea ash layers associated with ignimbrites. Geol. Mag. 117, 425–436.

Sparks, R.S.J., Walker, G.P.L., 1977. The significance of co-ignimbrite air-fall ashes associated with crystal-enriched ignimbrites. J. Volcanol. Geotherm. Res. 2, 329–341.

Sparks, R.S.J., Carey, S., Sigurdsson, H., 1991. Sedimentation from gravity currents generated by turbulent plumes. Sedimentology 38, 839–856.

Sparks, R.S.J., Bursik, M.I., Ablay, G., Thomas, R.M.E., Carey, S.N., 1992. Sedimentation of tephra by volcanic plumes: Part 2. Controls on thickness and grain-size variations of tephra fall deposits. Bull. Volcanol. 54, 685–695.

Stout, J.E., Arya, S.P., Genikhovich, E.L., 1995. The effect of nonlinear drag on the motion and settling velocity of heavy particles. J. Atmos. Sci. 52, 3836–3848.

Thorarinsson, S., 1967. The eruption of Hekla 1947–1948: I. The eruptions of Hekla in historical times. A Tephrochronological Study. Visindafelag Islendinga, Reykjavik, pp. 1–183.

Thorarinsson, S., Sigvaldason, G.E., 1972. The Hekla eruption of 1970. Bull. Volcanol. 36, 269–288.

Walker, G.P.L., 1973. Explosive volcanic eruptions—a new classification scheme. Geol. Rundsch. 62, 431–446.

Walker, G.P.L., 1980. The Taupo Pumice: product of the most powerful known (Ultraplinian) eruption. J. Volcanol. Geotherm. Res. 8, 69–94.

Walker, G.P.L., 1981a. Plinian eruptions and their products. Bull. Volcanol. 44 (2), 223–240.

Walker, G.P.L., 1981b. The Waimihia and Hatepe plinian deposits from the rhyolitic Taupo volcanic centre. N.Z. J. Geol. Geophys. 24, 305–324.

Wiesner, M.G., Wong, Y., Zheng, L., 1995. Fallout of volcanic ash to the deep South China Sea induced by the 1991 eruption of Mount Pinatubo (Philippines). Geology 23, 885–888.

Wilson, L., Huang, T.C., 1979. The influence of shape on the atmospheric settling velocity of volcanic ash particles. Earth Planet. Sci. Lett. 44, 311–324.